

Escaping Local Minima: A Finite-Time Markov Chain Analysis of Constant-Temperature Simulated Annealing

Hansini Ramachandran

*Department of Electrical and Computer Engineering
University of Southern California
Los Angeles, California
hramacha@usc.edu*

Bhaskar Krishnamachari

*Department of Electrical and Computer Engineering
University of Southern California
Los Angeles, California
bkrishna@usc.edu*

Abstract—Simulated Annealing (SA) is a widely used stochastic optimization algorithm, yet much of its theoretical understanding is limited to asymptotic convergence guarantees or general spectral bounds. In this paper, we develop a finite-time analytical framework for constant-temperature SA by studying a piecewise linear cost function that permits exact characterization. We model SA as a discrete-state Markov chain and first derive a closed-form expression for the expected time to escape a single linear basin in a one-dimensional landscape. We show that this expression also accurately predicts the behavior of continuous-state search up to a constant scaling factor, which we analyze empirically and explain via variance matching, demonstrating convergence to a factor of $\sqrt{3}$ in certain regimes.

We then extend the analysis to a two-basin landscape containing a local and a global optimum, obtaining exact expressions for the expected time to reach the global optimum starting from the local optimum, as a function of basin geometry, neighborhood radius, and temperature. Finally, we demonstrate how the predicted basin escape time can be used to guide the design of a simple two-temperature switching strategy.

I. INTRODUCTION

Simulated Annealing (SA) is a heuristic stochastic search algorithm that is widely used for many complex optimization problems ranging from Very Large Scale Integrated (VLSI) circuit placement and routing to quantum circuit compilation [8], [11]. It mimics the physical process of bringing a system to its minimum energy state by controlling its temperature.

While Simulated Annealing is empirically very successful, there are relatively fewer theoretical results characterizing its performance. Most prior results focus on steady state or asymptotic performance, or yield complex bounds that are not helpful for understanding finite state and time behavior.

To bridge this gap, this paper focuses on a simplified “toy model” of the energy landscape. While real-world objective functions are high-dimensional and non-convex, we believe that studying simpler idealized settings could allow for the derivation of exact mathematical expressions that reveal the underlying dynamics of the search process. Unlike prior literature that often focuses on cooling schedules, emphasizing simplicity to gain insights, our work prioritizes the relationship

between the geometric properties of the landscape and the expected hitting times under specific constant-temperature regimes.

Concretely, we present closed-form expressions for the behavior of constant-temperature SA in two discrete 1-D settings. First, we begin by analyzing a discrete 1-D piecewise linear function characterized by a single basin, and derive an expression for the expected time required for a constant-temperature SA process to exit the basin. We then demonstrate the robustness and wider applicability of this expression by applying it to a continuous version of the same function, identifying an empirical constant factor that converges to $\sqrt{3}$ under specific conditions.

Second, we analyze a dual-basin piecewise linear system that contains both a local and a global optimum. This extension allows us to formulate an expression for the expected time to reach the global optimum, providing a clear view of the dynamics of climbing out of a local optimum in the first basin to reach the global optimum in the second basin.

Third, we consider how the predicted first time to leave the suboptimal basin (obtained from our first analysis) could be used to determine an optimal time to switch from a high temperature to a low temperature. We show that this is indeed the case, finding empirically that the optimal switching time is generally monotonically increasing in the predicted mean time to leave the suboptimal basin (with an empirical quadratic fit offering a good regression).

These results serve as a foundational step toward a more rigorous, predictive theory of Simulated Annealing. By quantifying the interplay between temperature and landscape geometry in simple systems, we provide a framework that may eventually be scaled to higher-dimensional manifolds and gradual-temperature-reduction search processes, potentially guiding the development of more efficient self-tuning optimization algorithms.

II. RELATED WORK

The theoretical analysis of Simulated Annealing (SA) has progressed from asymptotic convergence guarantees to more

practical finite-time characterizations. Our work lies in the latter category: by restricting to simplified landscape geometries, we derive exact closed-form expected escape and hitting times that complement existing spectral bounds and diffusion-limit perspectives.

Early theory established global convergence under logarithmic cooling [4], and Hajek's critical depth framework [5] clarified that schedules must effectively be slower than the escape time from the deepest local minimum. We adopt the notion of basin depth but focus on finite-time, constant-temperature regimes and quantify the expected time to escape.

For finite-time behavior, spectral methods bound failure probability via the Markov chain's spectral gap [3], [7], which is closely related to metastability results where escape times scale exponentially with barrier height [6]. While these approaches yield rigorous general bounds, they often take the form of inequalities. By contrast, in idealized 1-D and two-basin toy landscapes—akin in spirit to piecewise-linear settings used to study mean first-passage times [9]—we obtain exact formulas that make the dependence on basin geometry (width and slope) and temperature explicit.

Our emphasis on constant temperature is also supported by prior work. Although adaptive strategies can offer speedups [1], Cohn and Fielding show that many landscapes admit an *optimal fixed temperature* minimizing expected hitting time to the global optimum [2]. Finally, the $\sqrt{3}$ scaling factor we observe when relating discrete random walks to continuous processes connects to optimal-scaling theory for Random Walk Metropolis: Roberts, Gelman, and Gilks analyze diffusion limits and motivate variance matching between uniform proposals and the continuous limit [10], which explains the discretization mismatch and our radius-rescaling correction.

III. SINGLE-BASIN ANALYSIS

A. Assumptions

Consider a one-dimensional, one-basin piecewise linear function (with a decreasing slope from $-N$ to 0, and with an increasing slope from 0 to N). We discretize the basin uniformly such that there are a total of $2N+1$ states where $\pm N$ are the absorbing boundaries.

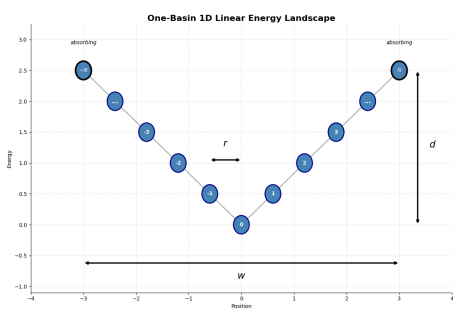


Fig. 1: Energy landscape for a linear 1-basin geometry with physical parameters labeled

For states $i \in \{1, \dots, N-1\}$:

$$P_{i,i+1} = p, \quad P_{i,i-1} = 0.5, \quad P_{i,i} = 0.5 - p$$

For states $i \in \{-N+1, \dots, -1\}$:

$$P_{i,i-1} = p, \quad P_{i,i+1} = 0.5, \quad P_{i,i} = 0.5 - p$$

For the center state $i = 0$:

$$P_{0,1} = P_{0,-1} = p, \quad P_{0,0} = 1 - 2p$$

The boundary (absorbing) states satisfy:

$$P_{-N,-N} = 1, \quad P_{N,N} = 1$$

B. Markov Chain / Random Walk Modeling

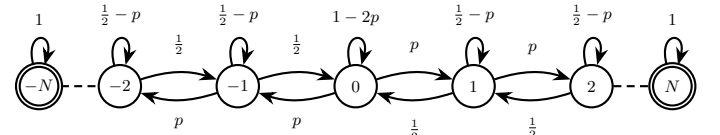


Fig. 2: Discrete Markov chain to model one linear basin with absorbing boundary states at $\pm N$.

The governing second order difference expression for the above Markov Chain is:

$$(0.5 + p)T_i - 0.5T_{i-1} - pT_{i+1} = 1 \quad (1)$$

The boundary condition is:

$$T_0 = 1 + pT_{-1} + pT_1 + (1 - 2p)T_0$$

Applying symmetry, we get $T_0 - T_1 = \frac{1}{2p} = \alpha$

To simplify the recurrence, define the first-difference sequence $b_i := T_i - T_{i+1}$, $i \geq 1$.

Rewriting equation (1) as a first order difference equation:

$$b_i = \frac{1}{p} + \alpha b_{i-1} \quad (2)$$

C. Derived Expression for Expected Time to Exit

Expressing equation (2) as a recursive sum and telescoping up to the absorbing boundaries, we obtain a closed-form expression for the expected time required to reach either absorbing state N or $-N$, starting from an arbitrary initial state i . The resulting estimate for the mean absorption time is given by

$$T_i = \sum_{k=i+1}^N \alpha^k + \frac{1}{p} \left[(N-i) \sum_{m=0}^{i-1} \alpha^m + \sum_{m=i}^{N-2} (N-m-i) \alpha^m \right] \quad (3)$$

where $\alpha = \frac{1}{2p}$.

The upward transition probability p may be expressed in terms of the underlying physical energy landscape. For the one-dimensional basin with a constant-slope piece-wise linear walls, where w denotes the basin width, r the maximum radius of a proposed move, d the basin depth, and T the temperature, the total number of discrete states is given by $N = \frac{w}{2r}$, and we can write $p = \frac{1}{2} \exp\left(\frac{-2rd}{wT}\right)$.

D. Fit to Continuous Case

The above formula for the estimated time to reach an absorbing boundary from a given interior state i was derived for a discrete random walk Markov chain. We can use this to also model a continuous Simulated Annealing random walk.

1) *Empirical results:* In this section, we explore the fit between the estimated mean time predicted by the formula in eq. (3) for a discrete piece-wise linear 1-basin landscape versus the average number of steps needed to reach an absorbing boundary from state 0 (center) with a continuous SA.

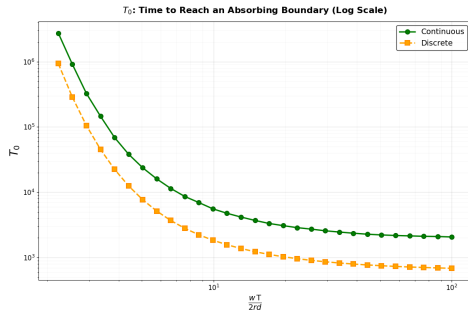


Fig. 3: Estimated time to absorption (continuous and discrete) from state 0 vs. $\frac{wT}{2rd}$ ratio

The dimensionless ratio $\frac{wT}{2rd}$ is varied from approximately 2.2 to 100 by adjusting the basin depth in Fig. 3. As the depth decreases and the basin becomes shallower, $\frac{wT}{2rd}$ increases, resulting in a reduced mean time to absorption. While both the continuous Metropolis-averaged random walk and the discrete theoretical prediction exhibit the same qualitative dependence on $\frac{wT}{2rd}$, their absolute values do not coincide exactly. This systematic discrepancy highlights the effect of discretization on the predicted absorption times, despite the underlying agreement in scaling behavior.

The relative error between the two estimates of T_i remains approximately constant, with a flat error level of about 67% across the parameter range considered. This behavior indicates that the discrepancy arises from a multiplicative bias, suggesting that the predicted and observed absorption times are related by a constant scaling factor. Applying a corrective factor to the radius, rather than rescaling absorption time directly, is preferable because discretization alters the effective step variance and therefore addresses the root cause of the mismatch rather than its outcome.

2) *Explanation of $\sqrt{3}$ limit:* Because the discrete theoretical expression consistently overestimates the observed mean absorption time, an empirical calibration was performed to identify an optimal radius scaling factor that aligns the analytical prediction with the Monte Carlo average computed over 2000 independent trials for identical physical parameters.

As $\frac{wT}{2rd}$ increases, the ratio between r_{cont} and r_{disc} converges asymptotically to $\sqrt{3}$. This factor arises from matching the effective drift and variance of the discrete random walk to those of its continuous diffusion limit. In the continuous

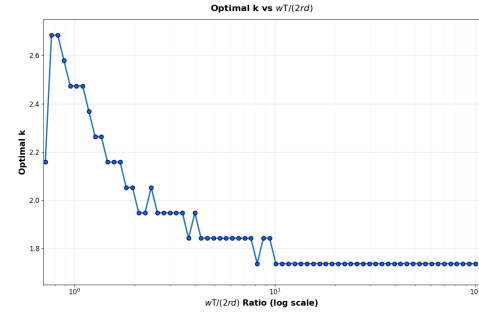


Fig. 4: Optimal k (radius scaling factor) vs. $\frac{wT}{2rd}$ ratio

Metropolis dynamics, the local motion can be approximated by a diffusion process whose infinitesimal variance is proportional to the second moment of the proposal distribution. In contrast, the discrete model uses a uniform proposal over a finite interval of width $2r_{\text{disc}}$, whose variance is $r_{\text{disc}}^2/3$. Matching this to the variance of the corresponding continuous diffusion therefore requires scaling the discrete proposal radius by a factor of $\sqrt{3}$, yielding $r_{\text{cont}} \approx \sqrt{3} r_{\text{disc}}$. In the regime of large $\frac{wT}{2rd}$, where boundary effects are negligible and the walk spends most of its time in the interior of the basin, this variance matching accurately captures the dominant contribution to the escape dynamics.

After radius scaling, the relative error remains below 7% in all but one of 100 trials, with a single outlier reaching 13%. This residual deviation arises from the stochastic nature of the process, as each data point represents an average over 2000 independent trials.

When $\frac{wT}{2rd}$ is small, the discrete walk overshoots the continuous walk more severely. In this regime, finite-step effects and interactions with the basin boundaries amplify the effective variance of the discrete dynamics, leading to faster-than-predicted escape and necessitating a larger correction factor $k > \sqrt{3}$.

With the proposal radius scaled by an optimal factor k , the relative error between $T_{0,\text{discrete}}$ and $T_{0,\text{continuous}}$ remains consistently below 9%. This level of agreement suggests that the discrete Markov-chain-based expression provides a reasonable approximation to the continuous mean first passage time T_0 across the parameter regimes considered. While the two models differ in their underlying state spaces, the observed correspondence indicates that the discrete formulation captures the primary dependence of the escape time on landscape geometry and temperature, making it a useful analytical reference for continuous simulated annealing in simplified settings.

IV. TWO-BASIN ANALYSIS

A. Setup

In this section, we extend the single-basin framework to model a more general energy landscape containing multiple local minima and a single globally optimal minimum (although the formulation naturally generalizes to multiple

optimal minima). The objective is to capture the dynamics of escape and convergence in the presence of competing basins, which more closely reflects realistic optimization landscapes. Unlike the single-basin case, the state space is now partitioned into two distinct basins separated by an energy barrier, and the effective slope within each basin need not be identical. This asymmetry introduces basin-dependent transition probabilities and escape rates, requiring separate characterization of the dynamics on either side of the barrier. While the underlying Markov structure and absorption framework remain unchanged, the two-basin model incorporates heterogeneous local geometry, enabling analysis of how basin depth and width jointly influence convergence behavior.

Consider a discrete Markov chain with two basins separated by a peak at M and an absorbing state at $N > M$. The state space is extended symmetrically to the left and consists of

$$-N, \dots, -M-1, -M, \dots, -1, 0, 1, \dots, M, M+1, \dots, N$$

where T_i denotes the expected hitting time of state N when starting from state i . The left boundary is reflecting, so that the dynamics for negative states are symmetric to those on the positive side, and in particular $T_{-i} = T_i$ for all $i \geq 1$.

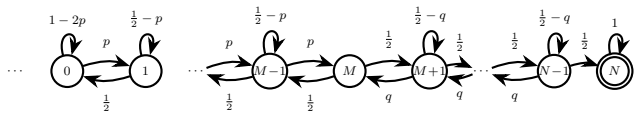


Fig. 5: Simplified representation of the two-basin Markov chain showing only the right-hand half of the state space. The omitted left-hand side consists of a reflected copy with identical transition structure. State M denotes the barrier between basins, and N is an absorbing state.

Left Basin ($1 \leq i \leq M-1$)

For states in the left basin, the transition probabilities are

$$P(i \rightarrow i+1) = p, \quad P(i \rightarrow i-1) = \frac{1}{2}, \quad P(i \rightarrow i) = \frac{1}{2}-p$$

where we take $p = \frac{1}{2} \exp(-2rd_1/(w_1T))$ for the left basin of width w_1 and depth d_1 .

Peak at M

At the barrier separating the two basins, transitions are unbiased:

$$P(M \rightarrow M-1) = \frac{1}{2}, \quad P(M \rightarrow M+1) = \frac{1}{2}.$$

Right Basin ($M+1 \leq j \leq N-1$)

Within the right basin, the transition probabilities are

$$P(j \rightarrow j-1) = q, \quad P(j \rightarrow j+1) = \frac{1}{2}, \quad P(j \rightarrow j) = \frac{1}{2}-q.$$

where we take $q = \frac{1}{2} \exp(-2rd_2/(w_2T))$ for a right basin of width w_2 and depth d_2 .

Absorbing State

The terminal state N is absorbing:

$$T_N = 0, \quad P(N \rightarrow N) = 1.$$

Symmetry at the local minimum (state 0)

At the point of symmetry, at state 0, the transition probabilities satisfy

$$P(0 \rightarrow 1) = p, \quad P(0 \rightarrow -1) = p, \quad P(0 \rightarrow 0) = 1-2p.$$

By symmetry, $T_{-i} = T_i$, so $T_{-1} = T_1$.

The first-step equation for T_0 is therefore

$$T_0 = 1 + (1-2p)T_0 + pT_1 + pT_{-1}$$

For the left basin (indices $0 \leq i \leq M$), define

$$D_i := T_i - T_{i+1}, \quad 0 \leq i \leq M, \quad (4)$$

Because the Markov chain is symmetric on both sides, we simplify and define the first difference as below with a boundary condition at state 0.

$$D_0 = T_0 - T_1 = \frac{1}{2p} \equiv \alpha.$$

$$D_i = \frac{1}{p} + \alpha D_{i-1}.$$

To replace the left basin recursion at the peak (state M),

$$D_M = 2 + D_{M-1}$$

For the right basin (indices $M \leq j \leq N-1$), define

$$B_j := T_j - T_{j+1}, \quad M \leq j \leq N-1. \quad (5)$$

We can write the difference equation for this basin as:

$$B_j = 2 + 2qB_{j-1}.$$

where q is the upward probability from states $M < j < N$ where the boundary condition for the landscape is

$$B_M = D_M.$$

B. Expression

The first-difference equations governing the left and right basins were solved using a common recurrence structure and a telescoping-sum argument. The boundary condition at the peak state was then applied to couple the two solutions, yielding a consistency relation between the left- and right-basin difference sequences D_i and B_j .

$$T_i = \begin{cases} \sum_{k=i}^{M-1} \left(\frac{1}{p} \sum_{j=0}^{k-1} \alpha^j + \alpha^{k+1} \right) + \sum_{s=0}^{R-1} \left(2 \sum_{u=0}^{s-1} \beta^u + \beta^s D_M \right) & 0 \leq i \leq M, \\ \sum_{s=i-M}^{R-1} \left(2 \sum_{u=0}^{s-1} \beta^u + \beta^s D_M \right) & M+1 \leq i \leq N-1. \end{cases}$$

where

$$D_M = 2 + \frac{1}{p} \sum_{j=0}^{M-2} \alpha^j + \alpha^M.$$

and

$$\alpha = \frac{1}{2p}; \beta = 2q$$

C. Empirical fit for the Continuous Case

To calibrate the discrete theoretical prediction against the averaged continuous-time absorption statistics, the same radius-scaling procedure was applied. In the two-basin setting, the correction factor was found to depend primarily on the dimensionless ratio $\frac{w_1 T}{2rd_1}$ associated with the suboptimal basin, provided that the optimal basin is sufficiently wide and deep ($\frac{w_2}{d} \gtrsim 5$). In this regime, the dominant source of discretization-induced mismatch arises from the suboptimal basin.

Here, the basin is sufficiently deep that once the walker crosses M , the probability of traversing back up the optimal basin rather than moving toward the minimum is very small. Consequently, changes in the proposal radius—affecting step size and local transition probabilities—do not accumulate through repeated stochastic retries. In other words, although the number of steps from M to N scales deterministically with $\frac{w}{2r}$, this dependence does not induce a multiplicative bias beyond the explicit geometric scaling already captured in the discrete model. As the ratio $\frac{w}{d}$ increases further, this already small multiplicative effect decreases rapidly. Empirically, it is observed that as long as $\frac{w_2}{d_2} \gtrsim 5$ (with the basin width also sufficiently large to yield a sufficient number of discrete states), the influence of the optimal basin on the fitted radius correction factor remains small. When this scaling factor k is applied, the relative error between the scaled discrete and continuous mean first passage times remains consistently below 5% over the corresponding range of $\frac{w_1 T}{2rd_1}$.

This suggests that, in this regime, the escape dynamics are primarily governed by the geometry of the suboptimal basin, and that the discrete formulation—after radius scaling—provides a reliable approximation to the continuous dynamics.

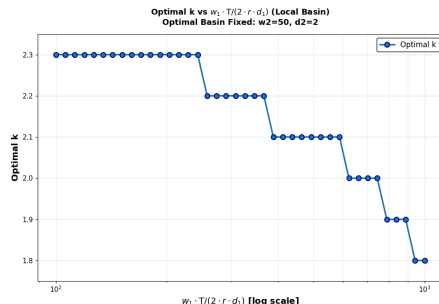


Fig. 6: Optimal k as a function of the ratio $\frac{w_1 T}{2rd_1}$, with the optimal-basin geometry held fixed at $w_2 = 50$ and $d_2 = 10$.

D. Exploration: Determining the Impact of Temperature

a) *Temperature*: We consider how the temperature impacts the hitting-time to reach the global optimum. Increasing T , which increases uphill acceptance (via larger p and q), is always better (i.e., monotonically reduces the hitting time), as seen in Fig. 10.

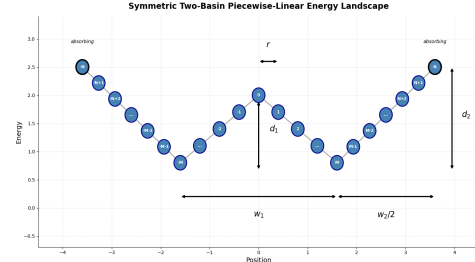


Fig. 7: Energy landscape for a linear 2-basin geometry with physical parameters labeled

The temperature is swept from $T = 1$ to $T = 50$ for several values of $\frac{w}{d}$ (3.5, 3.75, 4.0, and 4.25), while keeping the proposal radius fixed at $r = 1$. Only the discrete formula is used in this analysis.

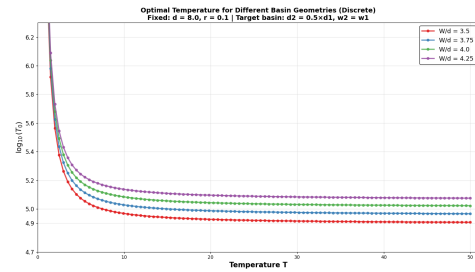


Fig. 8: Plot of mean first passage time vs. temperature for different basin geometries $\frac{w}{d}$

E. Finding an optimal time to switch temperature

An optimal switching time for a two-basin geometry arises from a basic trade-off in constant-temperature simulated annealing dynamics. At a higher temperature, uphill moves are accepted more readily, which increases the probability of escaping the suboptimal basin. However, maintaining a high temperature after the barrier has been crossed can be counterproductive: the chain continues to accept energetically unfavorable moves, increasing backtracking and reducing the tendency to reach the global minimum. Switching to a lower temperature after escape therefore can reduce T_0^{global} by ensuring the walker moves primarily downhill.

To illustrate the practical value of the closed-form escape-time prediction, we evaluate a simple two-temperature schedule that switches abruptly from a high temperature to a low temperature. Specifically, we fix $T_{\text{high}} = 10$ and $T_{\text{low}} = 3$, and we run SA at T_{high} for τ steps before switching to T_{low} for the remainder of the run. For each landscape configuration, τ is swept over a set of candidate values parameterized as $\tau = c \hat{t}_{\text{escape}}$, where \hat{t}_{escape} is the predicted mean time to

leave the local basin obtained from the discrete expression derived in Section III, and c is a scalar multiplier.

The dashed lines in Fig. 9 correspond to the baseline mean first-passage time T_0 when the temperature is held fixed at T_{high} throughout. In contrast, the two-temperature policy can reduce T_0 for an appropriate choice of τ , and the empirical results exhibit a clear minimizer over the tested multipliers c . This confirms that (i) a nontrivial optimal switching time exists for this setting, and (ii) the predicted local-basin escape time provides a useful scale for selecting the switching-time search range. In practice, the closed-form prediction can therefore be used to efficiently parameterize and narrow the exploration of switching policies, reducing the amount of empirical tuning required.

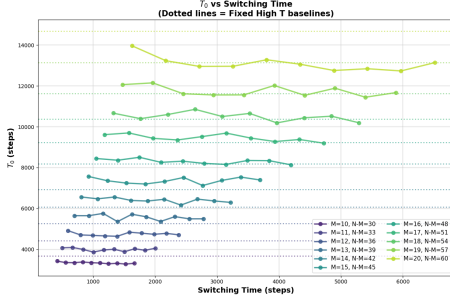


Fig. 9: Plot of mean first passage time for 2 basin geometry versus predicted switching time for different M/N basin configurations

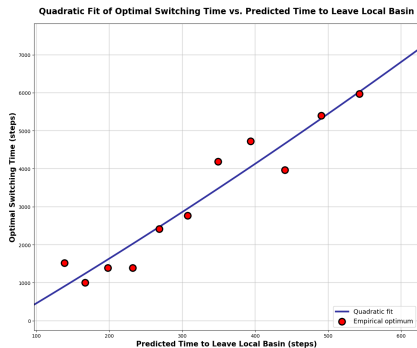


Fig. 10: Plot of optimal switching time versus predicted time to leave local basin with a quadratic line of best fit

The empirically determined optimal switching time τ is well approximated by a quadratic relation of the form $\tau = a_0 \hat{t}_{\text{escape}}^2 + a_1 \hat{t}_{\text{escape}} + a_2$, with fitted coefficients $a_0 = 2.31 \times 10^{-3}$, $a_1 = 11.09$, and $a_2 = -675.93$, yielding a coefficient of determination $R^2 = 0.924$.

This result indicates a superlinear dependence, well captured by a quadratic model over the range considered, between the optimal switching time from T_{high} to T_{low} and the predicted time to leave the local basin. Consequently, the predicted

basin escape time—which can be computed inexpensively from the discrete analytical expression—may be used to estimate an appropriate switching time without requiring repeated simulation-based tuning.

V. DISCUSSION AND FUTURE WORK

This paper is a preliminary step toward a predictive finite-time theory of Simulated Annealing. In simplified one-dimensional landscapes, we derived closed-form expressions for expected basin escape and hitting times under constant temperature. Although these toy models do not capture realistic high-dimensional structure, they provide analytical transparency and help isolate how landscape geometry and temperature govern finite-time performance.

Natural extensions include analyzing time-varying temperature schedules (e.g., multi-stage policies informed by estimated escape times) and moving beyond one dimension. While exact formulas may not persist in higher-dimensional or nonlinear landscapes, the approach here may still yield useful approximations or bounds, especially for separable structure or dominant escape pathways. Another direction is to study sequences or networks of basins, which better reflect practical energy landscapes. Finally, these closed-form predictions suggest a practical use: reducing empirical hyperparameter tuning by providing analytical guidance for temperature and proposal-scale selection. Testing how much tuning effort can be saved in practice is an important next step.

REFERENCES

- [1] O. Catoni. Rough large deviation estimates for simulated annealing: Application to exponential schedules. *The Annals of Probability*, 20(3):1109–1146, 1992.
- [2] H. Cohn and M. Fielding. Simulated annealing: searching for an optimal temperature schedule. *SIAM Journal on Optimization*, 9(3):779–802, 1999.
- [3] M. P. Desai and V. B. Rao. Finite-time behavior of slowly cooled annealing chains. *Probability in the Engineering and Informational Sciences*, 11(2):137–176, 1997.
- [4] S. Geman and D. Geman. Stochastic relaxation, gibbs distributions, and the bayesian restoration of images. *IEEE Transactions on Pattern Analysis and Machine Intelligence*, (6):721–741, 1984.
- [5] B. Hajek. Cooling schedules for optimal annealing. *Mathematics of Operations Research*, 13(2):311–329, 1988.
- [6] R. Holley, S. Kusuoka, and D. Stroock. Asymptotics of the spectral gap with applications to the theory of simulated annealing. *Journal of Functional Analysis*, 83(2):333–347, 1989.
- [7] D. Mitra, F. Romeo, and A. Sangiovanni-Vincentelli. Convergence and finite-time behavior of simulated annealing. *Advances in Applied Probability*, 18(3):747–771, 1986.
- [8] A. Molavi, A. Xu, E. Cecchetti, S. Tannu, and A. Albarghouthi. Generating compilers for qubit mapping and routing, 2025. arXiv:2508.10781v2.
- [9] V. V. Palyulin and R. Metzler. How a finite potential barrier decreases the mean first-passage time. *Journal of Statistical Mechanics: Theory and Experiment*, 2012(03):L03001, 2012.
- [10] G. O. Roberts, A. Gelman, and W. R. Gilks. Weak convergence and optimal scaling of random walk metropolis algorithms. *The Annals of Applied Probability*, 7(1):110–120, 1997.
- [11] C. Sechen and A. L. Sangiovanni-Vincentelli. The TimberWolf placement and routing package. *IEEE Journal of Solid-State Circuits*, 20(2):510–522, 1985.